Published in final edited form as:
Magn Reson Med. 2014 August ; 72(2): 316–323. doi:10.1002/mrm.24946.

In vivo detection of citrate in brain tumors by ^{1}H MRS at 3T

Changho Choi[1,2,3,*], **Sandeep K. Ganji**[1,2], **Akshay Madan**[1], **Keith M. Hulsey**[1], **Zhongxu An**[1,2], **Song Zhang**[4], **Marco C. Pinho**[1,2], **Ralph J. DeBerardinis**[5,6], **Robert M. Bachoo**[3,7,8,9], and **Elizabeth A. Maher**[3,7,8,9]

[1]Advanced Imaging Research Center, University of Texas Southwestern Medical Center, Dallas, Texas, USA

[2]Department of Radiology, University of Texas Southwestern Medical Center, Dallas, Texas, USA

[3]Harold C. Simmons Cancer Center, University of Texas Southwestern Medical Center, Dallas, Texas, USA

[4]Department of Clinical Sciences, University of Texas Southwestern Medical Center, Dallas, Texas, USA

[5]Children's Medical Center Research Institute, University of Texas Southwestern Medical Center, Dallas, Texas, USA

[6]McDermott Center for Human Growth and Development, University of Texas Southwestern Medical Center, Dallas, Texas, USA

[7]Department of Internal Medicine, University of Texas Southwestern Medical Center, Dallas, Texas, USA

[8]Department of Neurology and Neurotherapeutics, University of Texas Southwestern Medical Center, Dallas, Texas, USA

[9]Annette Strauss Center for Neuro-Oncology, University of Texas Southwestern Medical Center, Dallas, Texas, USA

Abstract

Purpose—To test whether the citrate is elevated in adult patients with gliomas using ^{1}H MRS at 3T *in vivo*.

Methods—Thirty-four adult patients were enrolled in the study, including 6 subjects with glioblastomas, 8 subjects with astrocytomas (5 WHO grade-3 and 3 grade-2), and 20 subjects with oligodendrogliomas (5 grade-3 and 15 grade-2). Five healthy volunteers were studied for baseline citrate data. Single-voxel localized spectra were collected with PRESS TE = 35 and 97 ms and analyzed with LCModel using numerically calculated basis spectra that include the effects of the PRESS radio-frequency and gradient pulses.

Results—Citrate was not measurable by MRS in healthy brain, but was detected in tumor patients at both echo times. The citrate concentration was estimated to be as high as 1.8 mM with reference to water at 42 M, with CRLB as low as 5%. The mean citrate level was 0.7±0.4 mM

[*]Correspondence to: Changho Choi, PhD, Phone: 214-645-2805, FAX: 214-645-2885, changho.choi@utsouthwestern.edu.

(mean±SD, n=32) with median CRLB of ~12%. No correlation was identified between citrate concentration and tumor grade or histological type.

Conclusion—Citrate was increased in the majority of gliomas in adult patients. The elevated citrate in our data indicates an altered metabolic state of tumor relative to healthy brain.

Keywords

citrate; gliomas; adults; ^{1}H MRS; 3T; PRESS (point-resolved spectroscopy); density-matrix simulation

INTRODUCTION

Tumors reprogram their metabolism to meet the needs of rapid cell growth and survival in harsh environments. Changes in metabolite abundance relative to normal tissue may serve as biomarkers of malignancy, and the ability to monitor these changes noninvasively would have significant clinical utility in cancer. Citrate (Cit) is positioned at a critical metabolic branch point, serving as an intermediate both for energy generation and for biosynthesis of lipids and related molecules (1,2). Therefore, perturbations in Cit abundance would reflect alterations in either the synthesis or utilization of this metabolite, and noninvasive analysis of Cit concentrations in tumors would provide a window into this important aspect of intermediary metabolism.

Citrate has four non-exchangeable protons from two magnetically equivalent CH_2 groups. The two protons of each group resonate in the proximity of 2.6 ppm with J coupling strength of ~15 Hz at neutral pH (3), giving rise to a dominant multiplet centered at 2.6 ppm. While Cit concentrations in prostate are normally high and *in vivo* detection of altered Cit levels by ^{1}H MRS is proven to be a useful tool for patient management in prostate cancer (4,5), Cit in the healthy human brain undergoes oxidation in the citric acid cycle and is not measurable by MRS *in vivo*. Prior ^{1}H MRS studies at 1.5T showed that Cit is significantly increased in pediatric tumors (6,7). We hypothesized that Cit may also be elevated in adult patients with gliomas. Detection of Cit in human brain by ^{1}H MRS is complicated by the presence of adjacent resonances of N-acetylaspartate (NAA) and aspartate (Asp) (8). Since the CH_2 proton resonances of NAA and Asp at ~2.6 ppm are all strongly coupled and spectrally distant from their weak-coupling partners, the signals are sensitive to MRS sequence parameters, such as inter-RF pulse delays and radio-frequency (RF) pulse bandwidth (9,10). Precise measurement of Cit in brain tumors therefore requires careful design of data acquisition and analysis.

In this article, we report elevation of Cit in adult patients with gliomas, as measured using single-voxel ^{1}H MRS at 3T *in vivo*. Two echo times (35 and 97 ms) of point-resolved spectroscopy (PRESS) were used for confirmation purpose, at which the Cit signals at 2.6 ppm have opposite polarity. Spectral fitting of the data was undertaken using numerically calculated spectra that include the effects of the volume-localized RF and gradient pulses as well as the subecho times. The performance of the data acquisition and analysis methods was validated in phantoms. Preliminary data for evaluation of Cit levels in various types of gliomas are presented.

METHODS

Thirty-four adult patients with gliomas (median age 36.5, range 20 – 62) were enrolled in this study. The study protocol was approved by the Institutional Review Board at the University of Texas Southwestern Medical Center and written informed consent was obtained prior to MR scans. The set of gliomas comprised 6 glioblastomas, 8 astrocytomas (5 grade-3 and 3 grade-2), and 20 oligodendrogliomas (5 grade-3 and 15 grade-2). The tumor types were determined by histology on biopsy, with World Health Organization criteria. In addition, 5 healthy volunteers (median age 32; range 25 – 36) were studied as controls.

Experiments were carried out on a whole-body 3T scanner (Philips Medical Systems, Best, The Netherlands). A body coil was used for RF transmission and an 8-channel phased-array head coil was used for signal reception. *In vitro* experiments were conducted on six spherical phantoms (6 cm diameter; pH = 7.0). The spectral patterns of Cit, NAA, and Asp were studied in three phantoms: one with Cit (22 mM) and creatine (Cr) (10 mM), one with NAA (30 mM), and one with Asp (33 mM) and Cr (10 mM). In addition, three phantoms were prepared for testing the Cit detectability in the presence of overlapping signals; (Cit, Asp, NAA) at (0, 19, 30), (5, 19, 30), and (0.7, 2, 3) mM. Data were obtained with PRESS TE = 35 and 97 ms sequences ((TE_1, TE_2) = (21, 14) and (32, 65) ms, respectively) and with STEAM (TE, TM) = (14, 19) ms from a 2×2×2 cm^3 voxel, using a TR of 12 s (number of signal averages (NSA) = 64). The PRESS and STEAM sequences used identically shaped 90° excitation RF pulses (9.8 ms; bandwidth = 4.2 kHz at half amplitude), whose amplitude/frequency modulations and excitation profiles are shown in a prior study (11). The PRESS TE = 35 and 97 ms sequences used 6.9 and 13.2 ms 180° pulses, respectively, whose bandwidths were both 1.3 kHz at an RF intensity (B_1) of 13.5 μT, as in a prior study (12). The transition width to bandwidth ratio of the 90° and the 6.9 and 13.2 ms 180° pulses were 9, 12 and 19%, respectively. The discrepancy between the STEAM and PRESS localized voxel shapes was ignored in the subsequent data analysis.

For *in vivo* scans in tumor patients, following survey imaging, T_2-weighted fluid-attenuated inversion recovery (T_2w-FLAIR) images were acquired to identify tumor masses. Spectra were acquired from a 2×2×2 cm^3 voxel positioned at the center of the tumor masses with NSA = 128. Data acquisition parameters included: TR = 2.0 s, spectral width = 2500 Hz, number of sampling points = 1024, and TE = 35 and 97 ms. First and second-order shimming was carried out, using FASTMAP (13). A vendor-supplied four-pulse variable-flip-angle sub-sequence was used for water suppression. Following each water-suppressed PRESS acquisition, an unsuppressed PRESS water signal was acquired using the same gradient scheme. In addition, an unsuppressed water signal was acquired from each voxel using STEAM (TE, TM) = (14, 19) ms and TR = 2 s. The multi-channel data were combined, with the scanner built-in routine, by summing the multi-channel data after correcting the zero order phase difference between channels using water reference data. For *in vivo* scans in healthy volunteers, data were acquired from the medial occipital lobes using the same parameters as in tumor scans.

Residual eddy current effects were minimized using the unsuppressed PRESS water signal. LCModel software (Version 6.3-0F) (14) was used for spectral fitting of metabolite and water data. The basis set included numerically simulated spectra of 21 metabolites, which included Cit, Asp, NAA, 2HG, NAAG, Glu, Gln, GABA, mI (myo-inositol), Gly (glycine), Lac (lactate), Cr (creatine + phosphocreatine), GSH (glutathione), Ala (alanine), Ace (acetate), Eth (ethanolamine), PE (phosphorylethanolamine), sI (*scyllo*-inositol), Tau (taurine), Glc (glucose), and Cho (glycerophosphorylcholine + phosphorylcholine). The LCModel built-in functions were used for fitting of macromolecule and lipid signals. The spectral fitting was conducted between 0.5 and 4.1 ppm. Cramér-Rao lower bounds (CRLB) were returned as percentage standard deviation by LCModel. Correlation coefficients between a pair of metabolite estimates, which are indicative of the interdependence of the signal estimates, were obtained from LCModel output files. Spectra with LCModel-returned FWHM (full width at half magnitude) less than 0.05 ppm were included in subsequent data analysis. Metabolite concentrations were estimated with reference to water at 42 M, ignoring potential differences of the water concentrations between tumors. For Cit, Cr, NAA and Cho, T_2 relaxation effects were corrected using the respective values of T_2 = 150, 150, 260, and 240 ms in healthy brain (15), and T_2 = 170, 170, 300, and 300 ms in tumors (16,17). T_1 was assumed to be the same for water and metabolites and in healthy brain and in tumors. Surgical cavities, areas of intratumoral hemorrhage, cystic changes and necrosis, identified on T_2w-FLAIR anatomical images, were excluded from the tumor voxels.

LCModel basis spectra of the metabolites were obtained, with an in-house Matlab program, for the PRESS and STEAM sequences used for data acquisitions. The time evolution of the density operator was calculated by solving the Liouville-von Neumann equation (18) for the Hamiltonian that includes the Zeeman, chemical shift and scalar coupling terms, and the slice-selective RF and gradient pulses. 3D volume localized metabolite spectra were calculated with a product-operator transformation matrix method, as described in our prior paper (Supplementary Information) (19). A transformation matrix, which represents the density operator evolution during an RF pulse, was created, for each slice-selective RF pulse of the PRESS and STEAM, with a spatial resolution of 1% (*i.e*. 0.01 = sample length / number of pixels / slice thickness). For the 180° pulses (bandwidth = 1.3 kHz), the sample length was two-fold greater than the slice thicknesses, thus with a carrier frequency at 2.7 ppm, spin resonances between −1.5 and 7 ppm were equally rotated through 180°. For the 90° pulse with bandwidth of 4.2 kHz, with a sample length to slice thickness ratio of 1.5 and the carrier frequency of 2.7 ppm, resonances between −4.5 and 10 ppm were equally excited. In addition, dual-echo spectra were calculated, using delta (1 ns) RF pulses tuned to 2.7 ppm (without volume localization) for comparison with the PRESS volume-localized simulations. Published chemical shift and J coupling constants (8,20) were used for the simulations.

One-way ANOVA analysis was performed to assess difference among tumor grades or histological types. The least square mean method was employed to estimate the mean and 95% confidence interval for each group. Statistical significance was declared for p-value < 0.05. All statistical analyses were conducted using software SAS 9.3 (SAS Institute, Gary, NC).

RESULTS

Phantom studies

Since the CH_2 proton multiplets of NAA and Asp overlap with the Cit signal and may interfere with Cit detection, we tested the LCModel fitting performance of our simulated basis sets of Cit, NAA and Asp in phantom data, Fig. 1. In the density matrix simulation of Cit, the four non-exchangeable protons of Cit were modeled as two AB spin systems with resonances (δ_A, δ_B) = (2.65, 2.54) ppm and a scalar coupling strength of J_{AB} = –15.1 Hz. For Cit, at TE = 35 ms, the phantom data showed that the strongly-coupled Cit spins produced a dominant signal at 2.6 ppm, with symmetric sidebands at 2.74 and 2.46 ppm. For a Cit to Cr concentration ratio of 2.2 (in Phantom-1 of Fig. 1), the Cit to Cr peak amplitude ratio was 1.22 when the spectra were broadened to have a Cr 3.03-ppm singlet linewidth of 4.3 Hz. The LCModel fits obtained with the PRESS volume-localization simulated basis sets (labeled Fit-1) and with delta RF pulse generated basis sets (labeled Fit-2) both reproduced phantom spectra at the short TE well, giving negligible residuals. In contrast to the positive multiplet of Cit at TE = 35 ms, the Cit signal at TE = 97 ms was a negative multiplet centered at 2.6 ppm. The calculated spectra for TE = 97 ms were somewhat different between the two simulation methods. While Fit-1 was essentially the same as the phantom spectrum, Fit-2 was slightly different from the experimental data, giving residual signals between 2.4 and 2.8 ppm. For the NAA and Asp CH_2 multiplets, the phantom spectra were also well reproduced by the Fit-1 (in Phantoms-2 and -3). However, Fit-2 was substantially different from the experimental data for both TEs, giving large residual signals. The discrepancy between Fit-2 and the phantom data was more extensive in the NAA CH_2 resonances than in the Asp CH_2 resonances, which was primarily due to the difference in the spectral distance between the CH_2 and CH resonances in NAA and Asp (1.8 *vs*. 1.2 ppm) with respect to the PRESS 180° pulse bandwidth (1.3 kHz).

The spectral analysis performance of the PRESS volume localized basis sets was further tested in composite phantoms, Fig 2. For the phantom with NAA and Asp only (Phantom-4), LCModel fitting gave zero Cit estimates at TE = 35 and 97 ms, while reproducing the prepared Asp and NAA concentrations. When the spectra were normalized to the NAA singlet amplitude, the composite phantoms that contained Cit (Phantoms-5 and -6) produced spectra with larger signals at 2.6 ppm than Phantom-4 and the spectrum with the largest signal at 2.6 ppm was from the phantom with the highest concentration of Cit relative to NAA and Asp (Phantom-6). Spectral fits reproduced the phantom spectra well. The prepared concentrations of Cit, NAA and Asp were reproduced by the fitting analysis within experimental errors (*e.g.*, 5%) in all three phantoms which included a case with potential *in-vivo* concentrations in tumors (Phantom-6). Asp and NAA gave signals at ~2.6 ppm, whose polarities were more or less positive at both TEs. For an NAA singlet linewidth of 4.3 Hz, the NAA CH_2 multiplet between 2.5 and 2.7 ppm was 10% and 6% with respect to the NAA CH_3 singlet amplitude at TE = 35 and 97 ms, respectively. In Phantom-5 ([Cit]/[NAA] = 1/6), the NAA CH_2 signal intensity was about the same as the Cit signal strength at TE = 35 ms, indicating approximately equal contributions of Cit and NAA to the phantom signal at 2.6 ppm. However, at TE = 97 ms, the negative signal at 2.6 ppm in the Phantom-5 and -6 spectra was solely due to the Cit signal since Asp and NAA both give positive signals.

Taken together, the composite signals of Cit, Asp and NAA were successfully resolved by spectral fitting with the PRESS sequence-specific calculated basis spectra.

Patient studies

In vivo brain spectra from a subject with oligodendroglioma (grade 3) are presented in Fig. 3a–b, together with voxel positioning in T_2w-FLAIR images and LCModel results for both PRESS TE = 35 and 97 ms, analyzed using PRESS volume-localized basis spectra. For validation purpose, residuals are presented of fitting with and without Cit in the basis set. MRS data were acquired from two locations; one in the superior and another in the inferior region of the tumor. The signal at 2.01 ppm was relatively small in both locations, indicating decreased NAA in the tumor. For the superior frontal region (Fig. 3a), the TE = 35 ms spectrum showed a signal at 2.6 ppm, which was greater than 10% of the NAA CH_3 singlet intensity. Spectral fitting gave a Cit concentration of 1.6 mM with a CRLB of 5%. A large negative signal was observed at 2.6 ppm in the TE = 97 ms spectrum, giving a Cit concentration of 1.8 mM following the correction for T_2 effects. Spectral fitting without Cit resulted in large residuals at ~2.6 ppm at both TEs, indicating that the signals at 2.6 ppm were primarily attributable to Cit. In contrast, the spectra from the inferior tumor region did not show a noticeable signal at 2.6 ppm at TE = 35 or 97 ms, giving very small Cit estimates with large CRLBs. Residuals for this region were essentially the same between the fittings with and without Cit. The Cit concentration was highly heterogeneous in the tumor, with the concentrations from 0 to 1.8 mM. For comparison, Cit was not measurable in healthy brain at TE = 35 or 97 ms, Fig. 3c. Residuals from the fitting with Cit were the same as those from the fitting without Cit.

Citrate was detected in several types of brain tumors, including oligodendroglioma, astrocytoma and glioblastoma. In each of the three cases in Fig. 4, a Cit signal was discernible at 2.6 ppm in the spectra and Cit was estimated to be higher than 0.5 mM with CRLB < 10%. The residuals were clearly different between the fittings with and without Cit when the Cit concentration was higher than 1 mM (Fig. 4a,b), but the residual difference was small in low Cit concentration cases (Fig. 4c). The classic pattern of elevated Cho with decreased NAA and Cr was observed in all gliomas. The strengths of the Cho, Cr and NAA signals were about the same in each of the three tumors. Lactate was elevated in the tumors.

Citrate was not measurable with acceptable precision in the five healthy subjects (medial occipital), Fig. 5. The Cit CRLB was between 53% and 999% at PRESS TE = 35 ms, and was 999% at PRESS TE = 97 ms, with citrate estimates of 0 – 0.1 mM. The mean value of the estimates was 0.03 and 0 mM from the TE = 35 and 97 ms data, respectively. For comparison, spectral fitting with delta-pulse generated basis spectra resulted in small CRLBs and high citrate estimates (i.e., 9 – 12% for the TE = 35 ms data, and 6 – 7% for the TE = 97 ms data, with a mean Cit estimate of ~0.8 mM), which are most likely misleading results primarily arising from the use of suboptimal basis multiplets of NAA and aspartate (Asp) for spectral fitting, as indicated in Fig. 1. From the TE = 35 and 97 ms data in the 5 controls, the concentrations of Cr, NAA, and Cho were estimated to be 7.6±0.8, 11.4±0.6, and 1.4±0.1 mM (mean±SD, n = 5). The FWHM values, returned from LCModel, were between 0.03 and 0.035 ppm.

Of the 34 tumor patients, data from 32 patients had LCModel-returned FWHM < 0.05 ppm at both TEs and were thereby selected for subsequent analysis (mean FWHM = 0.034±0.008 ppm). Spectral fitting was performed with PRESS volume-localized basis sets. The concentrations in these 32 glioma patients ranged from 0 to 1.8 mM with CRLB between 5 and 999% (Fig. 5). The mean concentration was estimated as 0.7±0.4 mM at both TE = 35 and 97 ms, but the median CRLB for TE = 35 ms data was slightly lower than that for TE = 97 ms (11% *vs*. 13%). Although Cit was not detected in some tumors (4 cases with CRLB > 50 at TE = 35 or 97 ms), the mean Cit estimate of the 32 tumors was significantly higher than the Cit level in healthy brain ($p = 2.0\times10^{-7}$, unpaired t-test). At both TEs, 21 tumors showed CRLB < 20% with mean Cit level at 0.9 mM, and 11 cases had CRLB < 10% with a mean Cit level of 1.2 mM. For the 32 tumors, the CRLBs of Cr, NAA and Cho were all ≤ 20%, the median values being 1 – 3%. The concentrations of Cr, NAA and Cho were estimated as 6.1±1.8, 3.2±1.6, and 3.0±1.2 mM, which were significantly different than in healthy brain ($p = 0.015$, 8×10^{-25}, and 5×10^{-5}), respectively. The estimates of Cit and Cr were both about the same for TE = 35 and 97 ms, indicating that a T_2 of 170 ms, which is a published T_2 of Cit in prostate (16), may be valid for correcting the Cit relaxation effects in brain tumors.

The LCModel analysis indicated that the Cit estimate was correlated with the Asp and NAA estimates, which is due to the spectral overlap of Cit with these metabolite signals. For the 32 tumor subjects, the correlation coefficients of Cit with NAA and Asp were −0.15±0.04 and 0.00±0.03 (mean±SD, n=32) for TE = 35 ms, and 0.02±0.03 and 0.14±0.09 for TE = 97 ms, respectively. The inverse correlation of Cit and NAA at TE = 35 ms was likely due to the same polarity (positive) of their signals at ~2.6 ppm and the positive correlation value of Cit and Asp at TE = 97 ms was likely due to the opposite polarity of the signals at ~2.6 ppm, as shown in Fig. 1. The correlation coefficients of Cit to metabolites other than NAA and Asp were essentially zero, which is not surprising since there was no considerable signal overlap with Cit.

The 32 gliomas included 20 oligodendrogliomas, 6 astrocytomas, and 6 glioblastomas, for which the mean estimated Cit concentrations were 0.7±0.4, 0.8±0.2, and 0.9±0.2 mM, respectively. One-way ANOVA analysis did not show a significant difference in mean Cit levels between the groups ($p = 0.73$). The Cho concentration, which is greater in tumors than in healthy brain, was 2.7±0.7, 4.0±1.7, and 3.2±1.3 mM in the three respective groups. The mean Cho level of the 20 oligodendrogliomas was significantly different from that of the 6 astrocytomas ($p = 0.01$), but there was no significant difference between the oligodendroglioma and glioblastoma groups ($p = 0.2$) or between the astrocytomas and the glioblastomas ($p = 0.4$). When the 32 tumors are grouped according to malignancy, there were 18 grade 2, 8 grade 3, and 6 grade 4 tumors, whose mean Cit levels were 0.6±0.3, 0.9±0.5, and 0.9±0.2 mM, respectively. There was a trend of high Cit levels in high grade tumors, but the ANOVA analysis did not indicate the presence of statistical significance ($p = 0.14$). Also, Cho was not significantly different between grades ($p = 0.11$).

DISCUSSION

The current paper reports the *in vivo* detection of Cit in adult patients with gliomas by ^{1}H MRS at 3T. PRESS TE = 35 and 97 ms methods were used for detection of the Cit signal at 2.6 ppm and the concentration was estimated with correction for the relaxation effects. Cit, which was not measurable in healthy brain in the present study or a prior study (6), was detected in many tumors. The mean concentration of Cit was approximately 0.7 mM, and the range of the concentration in individual patients was from 0 to 1.8 mM.

Although direct comparison of the results from the present study to those from a prior MRS study of pediatric tumors at 1.5T (7) may not be possible due to potential differences in quantification methods, the Cit estimate of the present study in adult patients is similar to the Cit level in indolent low-grade astrocytomas (0.6±0.8 mmol/Kg) but much lower than that in aggressive low-grade astrocytomas (4.1±1.1 mmol/Kg) (7). While there was no evidence of Cit elevation in pediatric glioblastomas (7), in the present study Cit was detected in all 6 adult patients with glioblastomas. Our data did not show correlation of Cit concentration with tumor type or grade.

In addition to Asp and NAA, NAAG, which was not included in our phantom study, has proton resonances in the proximity of 2.6 ppm. The aspartyl moiety of NAAG has coupled resonances at 2.52 and 2.72 and gives signals in the proximity of the Cit 2.6-ppm multiplet (20). Computer simulations indicated that, for identical concentrations of NAAG and Cit and a singlet linewidth of 4.3 Hz, the NAAG multiplet strength between 2.5 – 2.7 ppm is 18% and 9% relative to the Cit signal amplitude at TE = 35 and 97 ms, respectively. Given that NAAG was not observable in *ex vivo* tumor MRS studies (21), the spectral overlap of NAAG and Cit may not be a confounding factor in Cit detection in brain tumors. The presence of a negative signal at 2.6 ppm in PRESS TE = 97 ms spectra may be a conclusive indicator of elevated Cit as the signal is uniquely generated by Cit among known brain metabolites (7,8).

The numerical simulation results in Fig. 1 indicate that the pattern and intensity of the Cit multiplet at short TE is similar between volume-localized (PRESS) and hard pulse (non-volume localized) dual-echo sequences, but this is not the case at long TE. Further simulations of PRESS indicated that, at TE = 97 ms, 180° pulses with large bandwidth (10 kHz) gave a Cit signal very similar to that from the hard-pulse simulation. The intensity of the simulated Cit signal (when normalized to a singlet) decreased progressively with decreasing bandwidth. Thus, despite the small spectral distance between the Cit resonances, the Cit signal of long-TE PRESS has a dependence on the bandwidth of the 180° RF pulses. Also, long-TE PRESS Cit signals may be influenced by the transition width of the 180° refocusing profile. A simulation on a 3.4-ms 5-lobe 180° pulse, which had the same bandwidth (1.26 kHz) as the 180° pulses used in the present study but had a larger transition width to bandwidth ratio (37% *vs*. 9%), resulted in a reduced Cit signal at TE = 97 ms (*i.e.*, smaller by ~70%). As shown in Figs. 1 and 2, the CH_2 proton signals of NAA and Asp overlap with the Cit signal. Since the CH_2 protons for these metabolites are strongly coupled to each other and weakly coupled to their CH protons, the CH_2 multiplets at ~2.6 ppm produced by a PRESS sequence are sensitive to the 180° RF pulse bandwidth and transition

width. Thus, use of experimental RF and gradient pulse parameters for generating basis spectra for spectral fitting is critical for reliable measurement of Cit in brain tumors when the RF pulse bandwidths are not much greater than the spectral distance between the CH_2 and CH proton resonances of NAA and Asp. When the Cit concentration is high, Cit may be reliably measurable with proper basis spectra of metabolites. However, in cases with low Cit concentrations, the reliability of the measurement may be reduced due to the low signal-to-noise ratio of Cit and the effects of potential spurious signals and/or macromolecule signals at ~2.6 ppm, which could be fit into Cit.

Lastly, the biological basis for Cit elevation is unclear at present. It is also unclear why Cit accumulates in some adult brain malignancies and not others. In a recent *in-vivo* MRS study, ^{1}H signals from elevated Cit in pediatric glioma patients did not change over the course of a one-hour infusion of uniformly ^{13}C-labeled glucose, indicating that the Cit pool was not rapidly supplied by glucose carbon (22). Furthermore, early *ex-vivo* ^{13}C MRS studies revealed ^{13}C-labeled Cit following the infusion of ^{13}C-labeled acetate, but not after infusion of ^{13}C-labeled glucose (23–25). Both lines of evidence suggest that a significant fraction of citrate is produced from cells that can metabolize acetate. This would presumably include glial cells in the healthy brain, and perhaps acetate-metabolizing cells in a subset of adult gliomas. Given that Cit is not measurable by MRS in healthy brain, the presence of Cit on MRS may be a useful imaging marker in the diagnosis of brain malignancies. Further study will be required to determine whether Cit abundance is correlated with clinical symptoms or response to therapy.

Acknowledgments

This work was supported by US National Institutes of Health grants, R21CA159128 and R01CA154843, and by a Cancer Prevention Research Institute of Texas grant RP101243-P04. We acknowledge the technical helps from Dr. Ivan Dimitrov.

References

1. Mullen AR, Wheaton WW, Jin ES, Chen P-H, Sullivan LB, Cheng T, Yang Y, Linehan WM, Chandel NS, DeBerardinis RJ. Reductive carboxylation supports growth in tumour cells with defective mitochondria. Nature. 2012; 481:385–388. [PubMed: 22101431]
2. Icard P, Poulain L, Lincet H. Understanding the central role of citrate in the metabolism of cancer cells. Biochim Biophys Acta. 2012; 1825:111–116. [PubMed: 22101401]
3. Moore GJ, Sillerud LO. The pH dependence of chemical shift and spin-spin coupling for citrate. J Magn Reson B. 1994; 103:87–88. [PubMed: 8137073]
4. Barker, PB.; Bizzi, A.; De Stefano, N.; Gullapalli, RP.; Lin, DDM. Clinical MR Spectroscopy: Techniques and Applications. Cambridge: Cambridge University Press; 2010.
5. Hoeks CM, Barentsz JO, Hambrock T, Yakar D, Somford DM, Heijmink SW, Scheenen TW, Vos PC, Huisman H, van Oort IM, Witjes JA, Heerschap A, Futterer JJ. Prostate cancer: multiparametric MR imaging for detection, localization, and staging. Radiology. 2011; 261:46–66. [PubMed: 21931141]
6. Seymour ZA, Panigrahy A, Finlay JL, Nelson MD Jr, Bluml S. Citrate in pediatric CNS tumors? AJNR Am J Neuroradiol. 2008; 29:1006–1011. [PubMed: 18272551]
7. Bluml S, Panigrahy A, Laskov M, Dhall G, Krieger MD, Nelson MD, Finlay JL, Gilles FH. Elevated citrate in pediatric astrocytomas with malignant progression. Neuro Oncol. 2011; 13:1107–1117. [PubMed: 21771868]

8. Govindaraju V, Young K, Maudsley AA. Proton NMR chemical shifts and coupling constants for brain metabolites. NMR Biomed. 2000; 13:129–153. [PubMed: 10861994]
9. Kaiser LG, Young K, Matson GB. Numerical simulations of localized high field ^{1}H MR spectroscopy. J Magn Reson. 2008; 195:67–75. [PubMed: 18789736]
10. Choi C, Dimitrov IE, Douglas D, Patela A, Kaiser LG, Amezcua CA, Maher EA. Improvement of resolution for brain coupled metabolites by optimized ^{1}H MRS at 7 T. NMR Biomed. 2010; 23:1044–1052. [PubMed: 20963800]
11. Henning A, Fuchs A, Murdoch JB, Boesiger P. Slice-selective FID acquisition, localized by outer volume suppression (FIDLOVS) for ^{1}H-MRSI of the human brain at 7 T with minimal signal loss. NMR Biomed. 2009; 22:683–696. [PubMed: 19259944]
12. Choi C, Ganji S, Hulsey K, Madan A, Kovacs Z, Dimitrov I, Zhang S, Pichumani K, Mendnsohn D, Mickey B, Malloy C, Bachoo R, DeBerardinis R, Maher EA. A comparative study of short- and long-TE ^{1}H MRS at 3 T for in vivo detection of 2-hydroxyglutarate in brain tumors. NMR Biomed. (Published online 2013). 10.1002/nbm.2943
13. Gruetter R. Automatic, localized in vivo adjustment of all first- and second-order shim coils. Magn Reson Med. 1993; 29:804–811. [PubMed: 8350724]
14. Provencher SW. Estimation of metabolite concentrations from localized in vivo proton NMR spectra. Magn Reson Med. 1993; 30:672–679. [PubMed: 8139448]
15. Ganji SK, Banerjee A, Patel AM, Zhao YD, Dimitrov IE, Browning JD, Brown ES, Maher EA, Choi C. T2 measurement of J-coupled metabolites in the human brain at 3T. NMR Biomed. 2012; 25:523–529. [PubMed: 21845738]
16. Scheenen TW, Klomp DW, Wijnen JP, Heerschap A. Short echo time ^{1}H-MRSI of the human brain at 3T with minimal chemical shift displacement errors using adiabatic refocusing pulses. Magn Reson Med. 2008; 59:1–6. [PubMed: 17969076]
17. Madan, A.; Ganji, SK.; Maher, EA.; Choi, C. Measurement of transverse relaxation times in brain tumors. Proceedings of the 21th Annual Meeting of ISMRM; Salt Lake City, Utah, USA. 2013. p. 1997
18. Ernst, RR.; Bodenhausen, G.; Wokaun, A. Principles of nuclear magnetic resonance in one and two dimensions. Oxford: Clarendon Press; 1987.
19. Choi C, Ganji SK, Deberardinis RJ, Hatanpaa KJ, Rakheja D, Kovacs Z, Yang XL, Mashimo T, Raisanen JM, Marin-Valencia I, Pascual JM, Madden CJ, Mickey BE, Malloy CR, Bachoo RM, Maher EA. 2-hydroxyglutarate detection by magnetic resonance spectroscopy in IDH-mutated patients with gliomas. Nat Med. 2012; 18:624–629. [PubMed: 22281806]
20. Krawczyk H, Gradowska W. Characterisation of the ^{1}H and ^{13}C NMR spectra of N-acetylaspartylglutamate and its detection in urine from patients with Canavan disease. J Pharm Biomed Anal. 2003; 31:455–463. [PubMed: 12615232]
21. Wright AJ, Fellows GA, Griffiths JR, Wilson M, Bell BA, Howe FA. Ex-vivo HRMAS of adult brain tumours: metabolite quantification and assignment of tumour biomarkers. Mol Cancer. 2010; 9:66. [PubMed: 20331867]
22. Ashoori, I.; Panigrahy, A.; Nagasunder, A.; Dhall, G.; Nelson, MD.; Blüml, S. Dynamic proton MRS in pediatric brain tumors with prominent citrate. Proceedings of the 20th Annual Meeting of ISMRM; Melbourne, Australia. 2012. p. 1777
23. Badar-Goffer RS, Bachelard HS, Morris PG. Cerebral metabolism of acetate and glucose studied by ^{13}C-NMR spectroscopy. A technique for investigating metabolic compartmentation in the brain. Biochem J. 1990; 266:133–139. [PubMed: 1968742]
24. Badar-Goffer RS, Ben-Yoseph O, Bachelard HS, Morris PG. Neuronal-glial metabolism under depolarizing conditions. A ^{13}C-NMR study. Biochem J. 1992; 282:225–230. [PubMed: 1540138]
25. Bachelard HS, Badar-Goffer RS, Ben-Yoseph O, Morris PG, Taylor A, Thatcher N. ^{13}C-MRS studies on cerebral metabolism. MAGMA. 1994; 2:285–289.

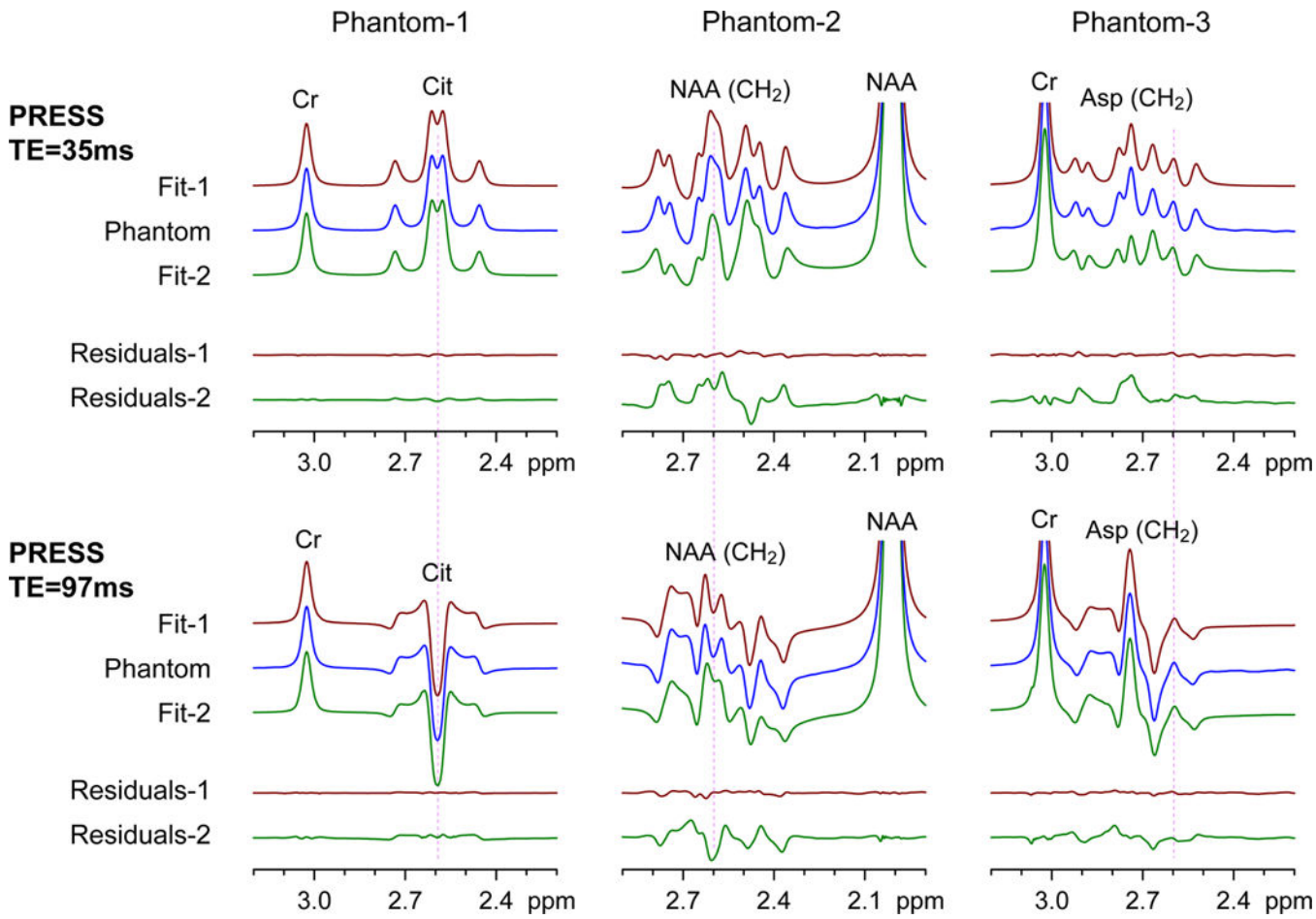

FIG. 1.

Phantom spectra of Cit (Phantom-1), NAA (Phantom-2), and Asp (Phantom-3), obtained with PRESS TE = 35 and 97 ms at 3T, are shown together with LCModel fitting results. The spectral fitting was undertaken with basis spectra that were calculated using the PRESS volume-localization RF and gradient pulses (Fit-1 and Residuals-1) and using 1-ns (non-localizing) 90° and 180° RF pulses (Fit-2 and Residuals-2). Residuals represent subtraction of calculated spectra from phantom spectra. Spectra were broadened to have singlet linewidths (FWHM) of 4.3 Hz prior to LCModel fitting. Spectra are normalized to the Cr or NAA singlet amplitude. A vertical line is drawn at 2.6 ppm.

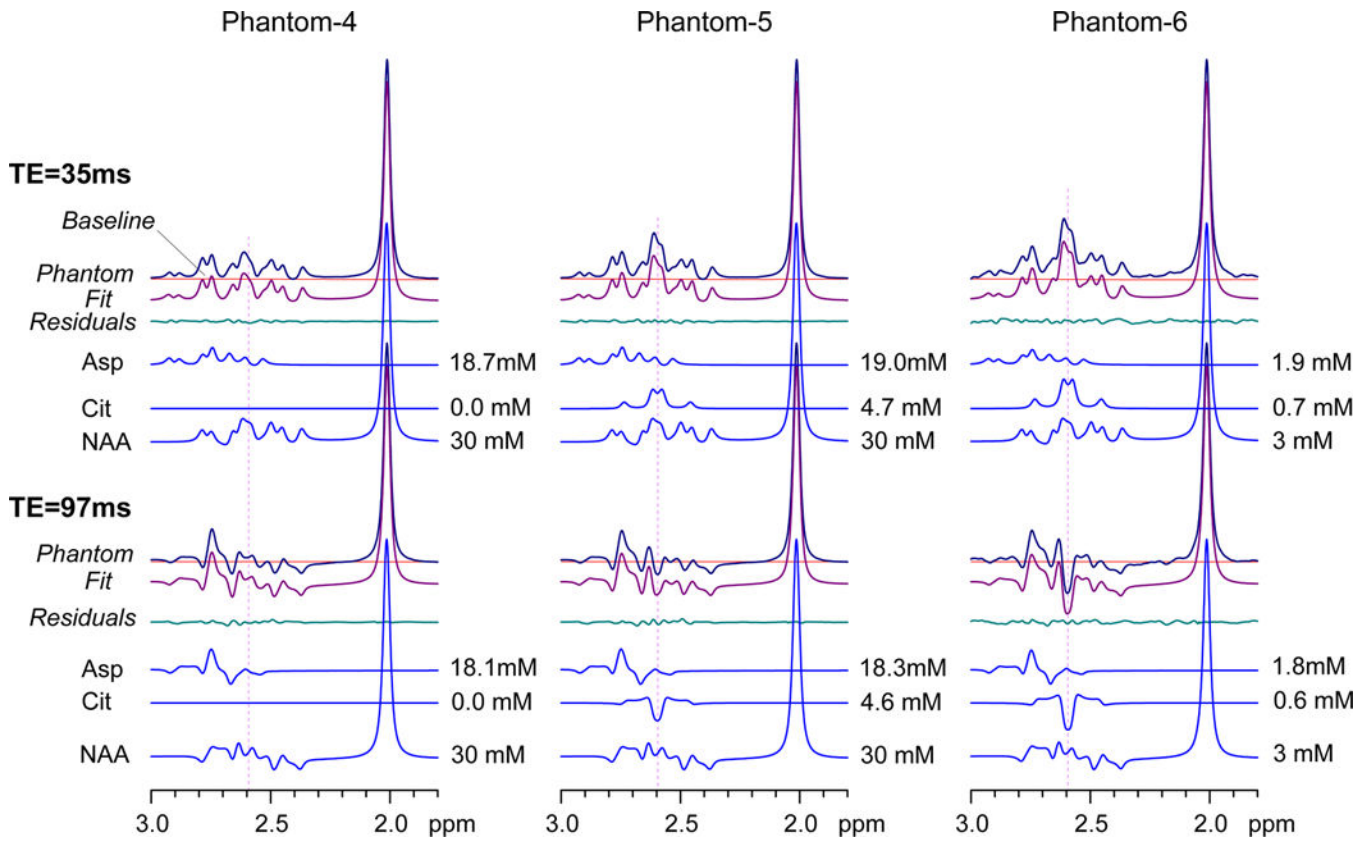

FIG. 2.

Spectra at 3T from three composite phantom solutions are displayed with LCModel fits and residuals for PRESS TE = 35 and 97 ms. PRESS volume-localized basis spectra were used for spectral fitting. The signals of Asp, Cit and NAA are shown with concentration estimates. Phantom-4, -5, and -6 were prepared for (Cit, Asp, NAA) at (0, 19, 30), (5, 19, 30), and (0.7, 2, 3) mM, respectively. Spectra were broadened to NAA singlet linewidth of 4.3 Hz and normalized with respect to the NAA singlet amplitude.

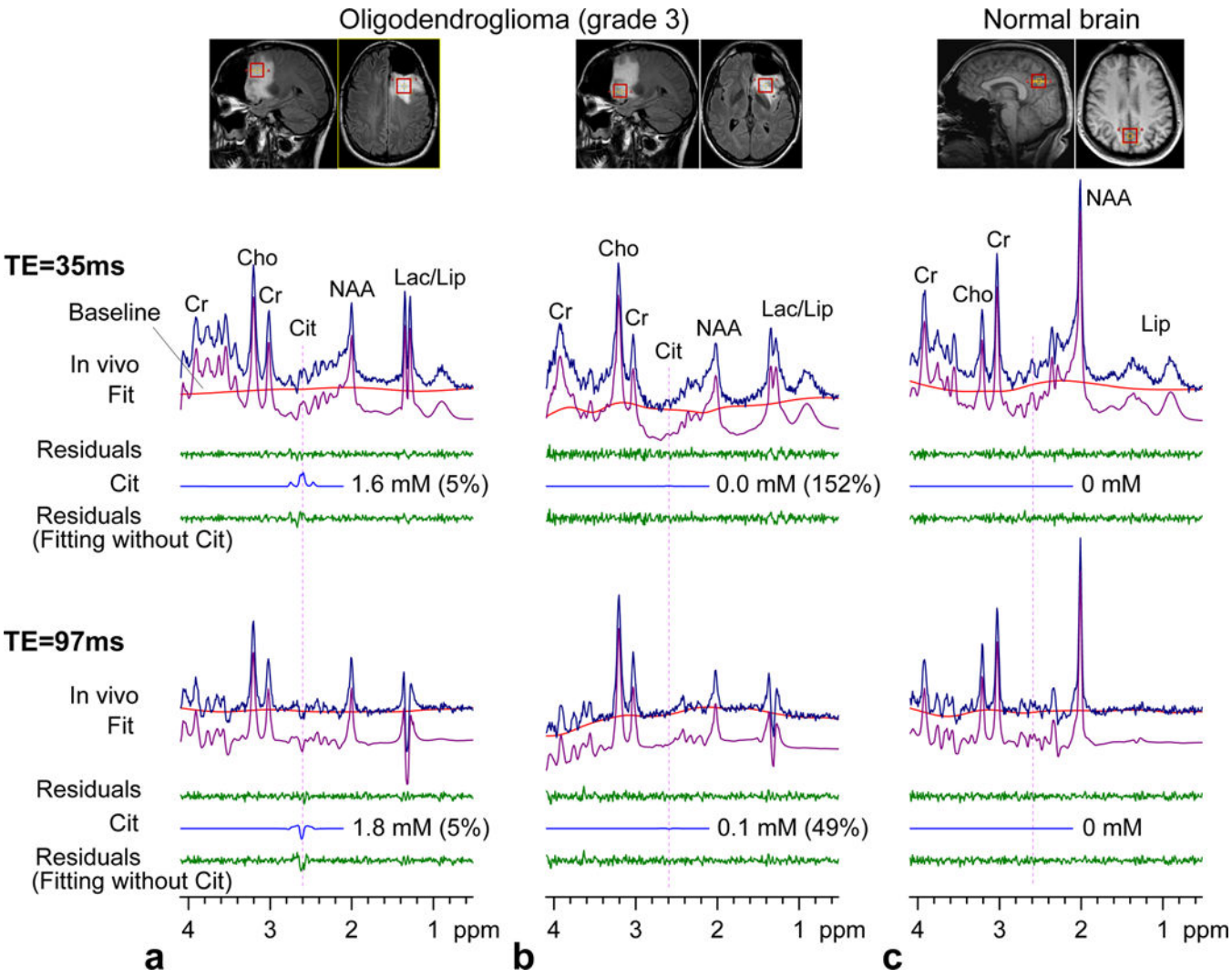

FIG. 3.

In vivo brain spectra at 3T from a patient with oligodendroglioma and a healthy volunteer are shown together with LCModel fits and residuals for PRESS TE = 35 and 97 ms. PRESS volume-localized basis spectra were used for spectral fitting. The Cit signal is shown with the concentration and CRLB of Cit. The lower trace of each *in vivo* spectrum shows residuals from the LCModel fitting with a basis set without Cit. The patient was scanned for two locations post-surgery. The voxel size was 2×2×2 cm^3 (TR = 2 s; NSA = 128). Each spectrum was normalized with respect to the short-TE STEAM water signal from the voxel.

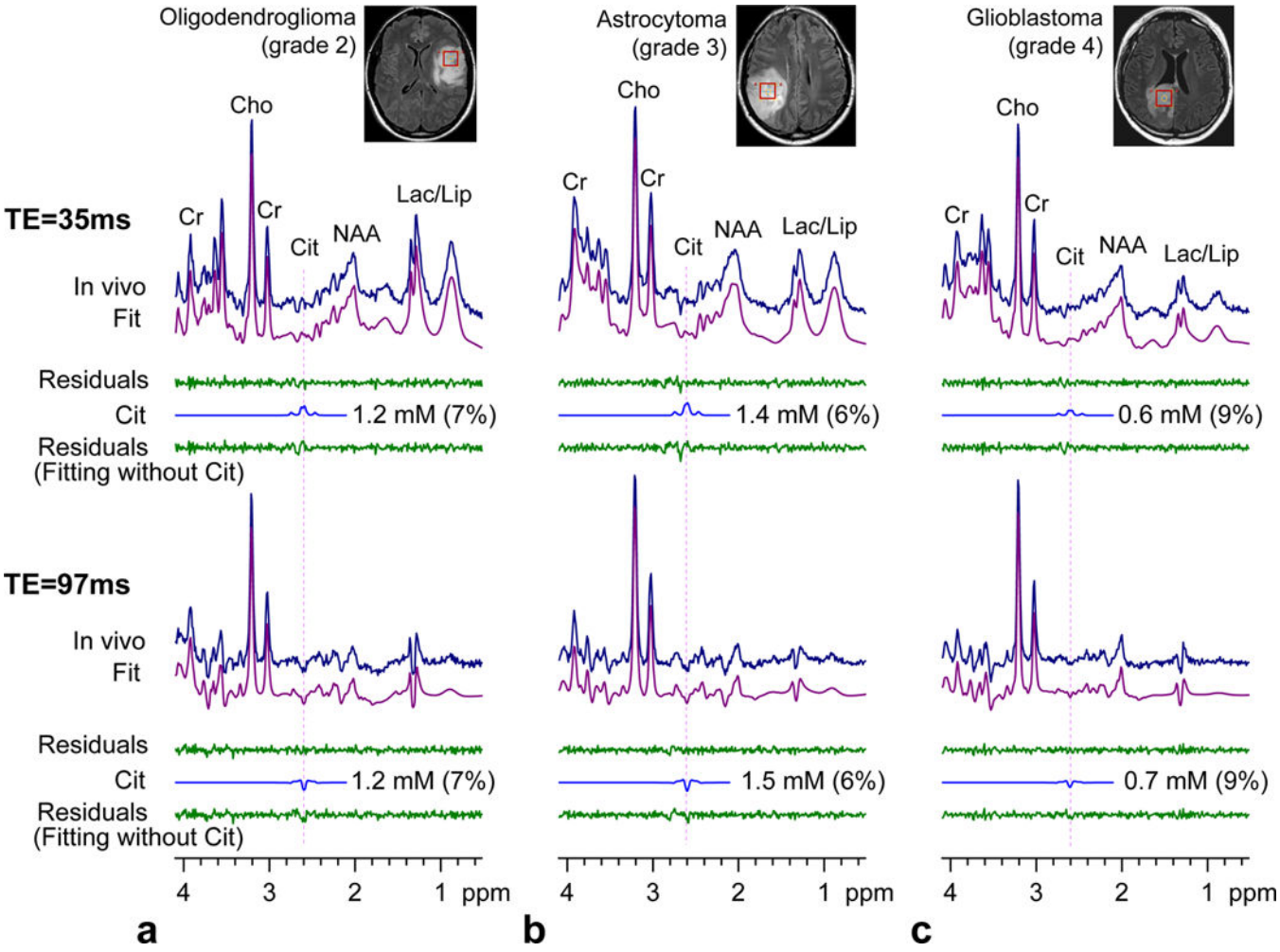

FIG. 4.

In vivo spectra from 3 subjects with gliomas, obtained with PRESS TE = 35 and 97 ms at 3T, are shown together with LCModel fits, residuals, and the Cit signals. The Cit concentration estimate and CRLB are presented for each patient. Data are shown in a similar manner as in Fig. 3.

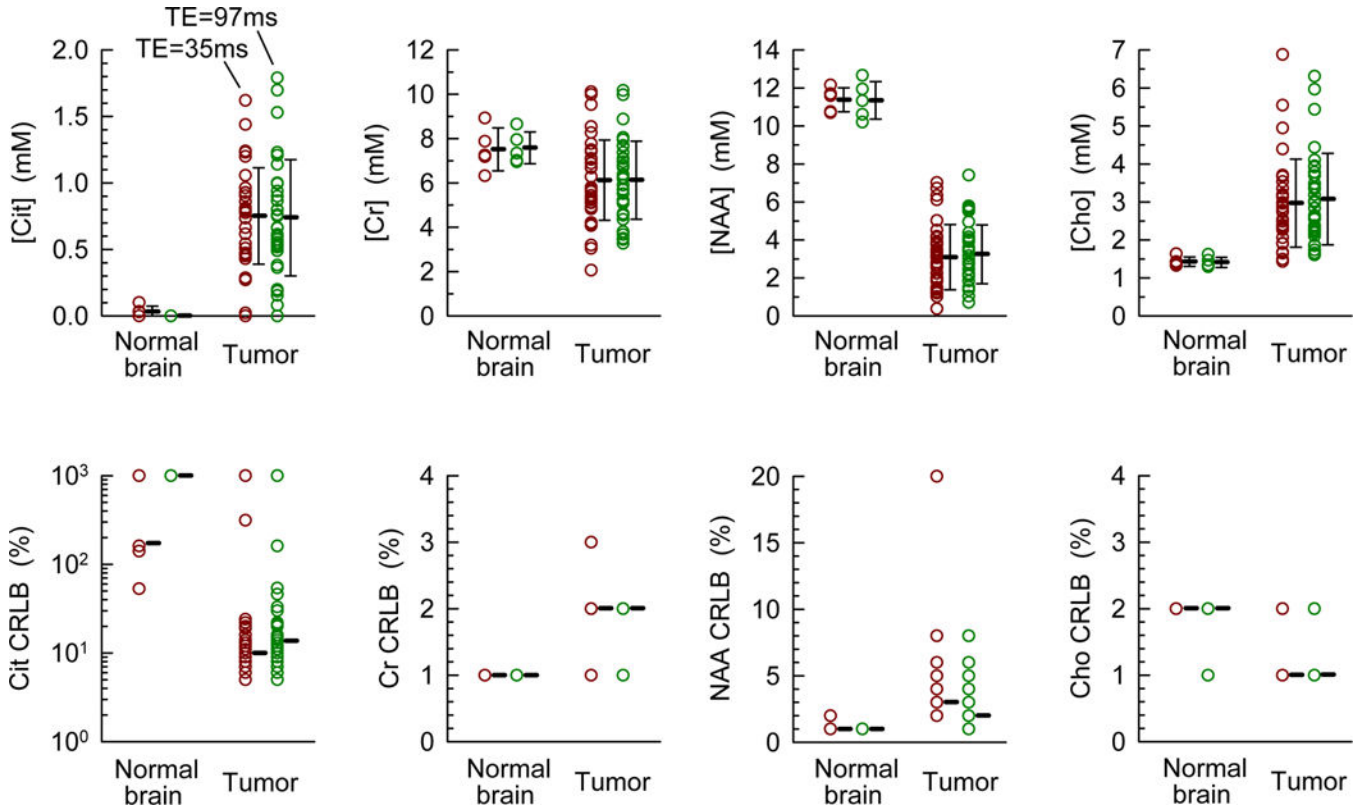

FIG. 5.

Concentrations and CRLBs of Cit, Cr, NAA, and Cho in 5 healthy volunteers and 32 adult patients with gliomas, obtained with PRESS TE = 35 and 97 ms are shown here. In the upper panel, the error bars represent the standard deviation of the concentration with respect to the mean values which are indicated by thick bars. The median value of the integer CRLBs (returned by LCModel) is shown as a bar in the lower panel.